nature communications

Article

https://doi.org/10.1038/s41467-026-72864-0

Operating a non-Hermitian atomic magnetometer with programmable digital electronics

Received: 18 September 2025

Accepted: 20 April 2026

Published online: 07 May 2026

Check for updates

Tianyu Qian[1,2,12], Jipeng Xu[1,3,4,12], Ran Huang[5], Keyu Xia[6,7], Zhiqiang Xiong[8], Hongchang Zhao[1,2], Chao Wang[1,2], Yuchen Feng[1,2], Jintao Zheng[1,2], Jiajia Li[1,2], Hui Luo[1], Shiqiao Qin[1], Franco Nori[5,9], Hui Jing[10,11] & Zhiguo Wang[1,2]

Non-Hermitian systems with exceptional points (EPs) have attracted much attention for their potential to increase sensitivity. However, EPs are difficult to generate and control accurately in most physical systems, as they are extremely sensitive to environmental disturbances. We propose a unique non-Hermitian system formed by hybridizing digital electronics with physical sensors. The programmability of digital electronics allows EPs to be created, manipulated, and applied easily and flexibly. More interestingly, the modular design of our system facilitates coupling with various physical sensors, increasing their linear response to an EP-enhanced sublinear response. By coupling digital electronics with an atomic magnetometer, we achieved a 4.27-fold sensitivity increase for weak magnetic field measurements. Our work opens a new frontier at the junction of three active fields, namely, atomic physics, electronics, and non-Hermitian devices. The programmability, scalability, and practicality of our approach could further increase the universality, complexity, and intelligence of non-Hermitian fields.

Sensor performance is mainly limited by loss during signal transmission, such as mirror reflection loss in optical cavities, friction loss in mechanical oscillators, and depolarization and decoherence (inherent loss) in atomic vapor cells. Traditional methods usually suppress these losses through the optimization of fabrication processes or the use of innovative structures, but overlook the potential for loss control. In recent years, sensing enhancement based on exceptional points (EPs) in non-Hermitian systems has shown the potential to increase measurement sensitivity[1–7]. The principle underlying the use of non-Hermitian systems to increase sensor sensitivity fundamentally differs from traditional approaches. When a non-Hermitian Hamiltonian traverses an EP in parameter space, the simultaneous degeneracy of both eigenvalues and eigenstates occurs, whereas in Hermitian systems, only eigenvalue degeneracy arises, with eigenstates remaining

[1]College of Advanced Interdisciplinary Studies, National University of Defense Technology, Changsha, China. [2]Hunan Key Laboratory of Mechanism and Technology of Quantum Information, National University of Defense Technology, Changsha, China. [3]Hunan Provincial Key, Laboratory of Novel Nano-Optoelectronic Information Materials and Devices, National University of Defense Technology, Changsha, China. [4]Frontiers Science Center for Nano-optoelectronics and State Key Laboratory for Mesoscopic Physics, School of Physics, Peking University, Beijing, China. [5]Quantum Information Physics Theory Research Team, Center for Quantum Computing (RQC), RIKEN, Saitama, Japan. [6]College of Engineering and Applied Sciences, National Laboratory of Solid State Microstructures, Nanjing University, Nanjing, China. [7]Shishan Laboratory, Suzhou Campus of Nanjing University, Suzhou, China. [8]Huaguan Technology Co. Ltd., Changsha, China. [9]Physics Department, The University of Michigan, Ann Arbor, MI, USA. [10]Key Laboratory of Low-Dimensional Quantum Structures and Quantum Control of Ministry of Education, Department of Physics, Hunan Normal University, Changsha, China. [11]Institute for Quantum Science and Technology, College of Science, National University of Defense Technology, Changsha, China. [12]These authors contributed equally: Tianyu Qian, Jipeng Xu.
e-mail: luohui.luo@163.com; shiqiaoqincn@163.com; jinghui@hunnu.edu.cn; maxborn@nudt.edu.cn

orthogonal[8]. This process is accompanied by a sublinear response enhancement scaling as $\varepsilon^{\frac{1}{N}}$ (where ε denotes the perturbation strength and N is the system dimension)[9–11]. Thus, non-Hermitian systems can utilize loss to enhance the signal near the EPs[12–16]. Such enhancement mechanisms have been experimentally validated in optical[17–23] and electronic platforms[24–28], demonstrating performance improvements in displacement sensing[25,26,29,30], thermal metrology[31], inertial measurement[13,32], and acceleration detection[33]. Moreover, non-Hermitian systems have also been used to study exceptional quantum effect[34], loss-induced chirality inversion[35], and spin-selective topological effects[36].

The implementation of non-Hermitian EP sensing in most systems often faces inherent limitations. The extreme sensitivity near EPs leads to fragile couplings, making gain-loss and phase control difficult to achieve simultaneously and prone to introducing excess noise[37–41]. In contrast to most physical samples, digitally synthesized non-Hermitian sensing systems exhibit increased tuning flexibility with reduced control complexity. However, no attempts have been made to integrate a physical non-Hermitian EP system with digital electronics to realize high-dimensional parameter control and ultrasensitive measurements. Furthermore, although EP sensitivity enhancement has been observed in electronic circuits[33], optical resonators[42], and magneto-optical media[43], this phenomenon demands rigorous verification in additional physical architectures[19,39,44–48].

In this study, a method of coupling digital electronics with physical systems is proposed, and the establishment of resonant coupling between digital electronics and a physical sensor is explored, in which an EP-enhanced magnetometer is constructed. In this hybrid architecture, the atomic magnetometer (AM) unit enables ultrasensitive weak magnetic field detection, whereas the digital electronic (DE) unit enables real-time parametric control near EPs. Leveraging the high-precision and high-dimensional control capabilities of digital electronics, the combined system enables simultaneous manipulation of phase and gain while implementing relative noise suppression during measurements. The maximum response and sensitivity achieved by this prototype are 4.52 times and 4.27 times greater than those of a conventional AM, respectively. The modular architecture permits direct substitution of the AM unit with alternative sensing elements, such as an optical force sensor[49], a microelectromechanical system (MEMS) gyroscope[50], and a nitrogen-vacancy (NV) center magnetometer[51], considerably increasing the applicability of the proposed system. The programmability of the DE unit would facilitate further research in which the hybrid system is combined with artificial intelligence (AI) algorithms, such as deep learning and evolutionary computation methods, to promote the application of non-Hermitian physics in various classical and quantum measurements.

Results

Hybrid non-Hermitian system

The hybrid non-Hermitian system is shown in Fig. 1a. The AM unit is used as a sensor with inherent loss for detecting the magnetic field (B_z) by measuring the Larmor precession frequency of atoms (specific details are provided in the “**Methods**” section). The DE unit, which serves as an EP generator, regulates the loss, gain, and coupling of the system. Specifically, the atomic precession signal enters the computer, couples with the digital resonator, and is fed back to both the digital resonator and the atoms, completing non-Hermitian control.

This control strategy leverages the loss characteristics of the system, which were originally intended to be suppressed, representing a new approach to enhancing measurement capabilities. The hybrid system introduces gain feedback and energy exchange between subsystems, in addition to the inherent losses in the AM (Fig. 1b, c). As shown in Fig. 1c, after the introduction of the non-Hermitian control strategy, the response transforms from a simple linear response to an EP-enhanced response. Our platform enables in situ reconfiguration between the EP and non-EP regimes via dynamic toggling of the coupling.

As the eigenvalue variation near the EP shifts from linear to sublinear, the system response is amplified. Figure 1d presents experimental measurement results for the non-Hermitian magnetometer before and after coupling. The coupled system demonstrates a significantly enhanced response for both DC and AC signals.

The AM unit in the system can be described by the Bloch equations:

$$\begin{aligned}\dot{M}_x &= \omega_y M_z - \omega_z M_y - M_x/T_2,\\ \dot{M}_y &= \omega_z M_x - \omega_x M_z - M_y/T_2,\\ \dot{M}_z &= \omega_x M_y - \omega_y M_x - (M_0 - M_z)/T_1.\end{aligned} \tag{1}$$

Where $M_{x,y,z}$ are the projections of the atomic magnetization vector $\vec{\mathbf{M}}$ on the x, y and z axes, $\omega_{x,y,z} = \Gamma B_{x,y,z}$ is the atomic precession frequency about the x, y and z axes, and Γ is the atomic gyromagnetic ratio, T_1 and T_2 are the longitudinal and transverse relaxation times of the atom, respectively. We denote $y_1 = M_+ = M_x - iM_y = M_\perp \bullet e^{i\varphi}$ as the signal output of the atoms, and $x_1 = M_z\,\omega_x = M_z\,\Gamma B_x$ as the signal input caused by the magnetic field B_x from the x-axis coil. Here, $\omega_z = \omega_1$ represents the eigenfrequency of atomic precession, $1/T_2 = \gamma_1$ indicates the loss, and $\omega_y = 0$ signifies no input along the y-axis. Assuming M_z remains constant during the experiment, Eq. (1) can be rewritten as follows:

$$\dot{y}_1 = -(i\omega_1 + \gamma_1)y_1 + ix_1. \tag{2}$$

The DE unit is a one-dimensional digital resonator simulated by a computer, which can be described by the following differential equation:

$$\ddot{y}_2 + 2\gamma_2\dot{y}_2 + \omega_2^2 y_2 = 2\gamma_2\omega_2 x_2, \tag{3}$$

here, x_2 and y_2 represent the input and output of DE unit, ω_2 is the eigenfrequency, and γ_2 is the loss. After applying approximation and order reduction to Eq. (3), we obtain:

$$\dot{y}_2 = -(i\omega_2 + \gamma_2)y_2 + ix_2. \tag{4}$$

Next, as shown in Fig. 1a, we linearly add their outputs and use the result as the system input, thus obtaining $x_n = g_n(\kappa_1 e^{-i\theta} y_1 + \kappa_2 e^{-i\varphi} y_2)$. Here $e^{-i\theta}$ and $e^{-i\varphi}$ are phase-shift factors and κ_1, κ_2, g_1, and g_2 are gain factors, all of which can be tuned in the computer simulation. Finally, by defining $\boldsymbol{\Psi} = (y_1\, y_2)^{\mathrm{T}}$, the system of equations can be written in a Schrödinger-like form, namely $\dot{\boldsymbol{\Psi}} = -iH_{eff}\boldsymbol{\Psi}$, where the effective Hamiltonian is given by:

$$\widehat{H}_{eff} = \begin{bmatrix} \Delta\omega - i\gamma_1 - g_1\kappa_1 e^{-i\theta} & -g_1\kappa_2 e^{-i\varphi} \\ -g_2\kappa_1 e^{-i\theta} & -\Delta\omega - i\gamma_2 - g_2\kappa_2 e^{-i\varphi} \end{bmatrix}, \tag{5}$$

where $\Delta\omega$ is the eigenfrequency difference between atoms and the digital resonator. Additionally, the Hamiltonian contains phase shift factors $e^{-i\theta}$ and $e^{-i\varphi}$ and gain factors κ_1, κ_2, g_1, and g_2. Similarly, the eigenvalues contain these parameters, providing a diverse way to generate and control the hybrid EPs. Changing B_z alters the atomic eigenfrequency, and adjusting the phase and gain modules alters the gain and energy exchange of the hybrid system, which is crucial for controlling the hybrid EPs (The complete derivation process of the Hamiltonian is detailed in the Supplementary Materials).

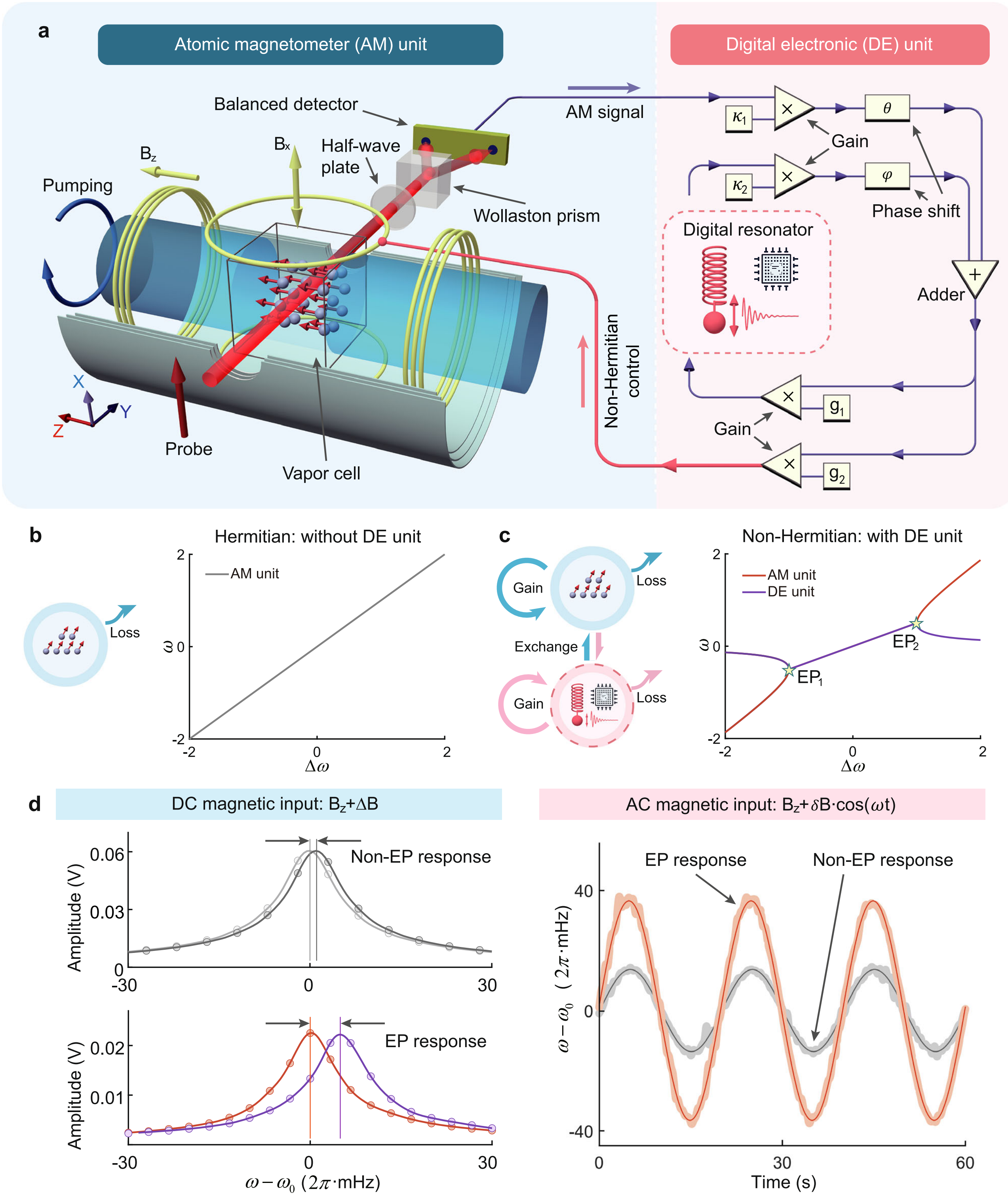

Fig. 1 | Hybrid EP-enhanced magnetometer. a Schematic of the hybrid EP-enhanced magnetometer, consisting of an atomic magnetometer (AM) unit and a digital electronic (DE) unit. The AM unit includes an atomic vapor cell, pump light, probe light, magnetic field coils, and detector. The DE unit is composed of a digitally simulated resonator and gain and phase shift modules. The gain module is implemented by a multiplier, the phase shift module is implemented by a shift register, and the signal coupling is performed by an addition operation. The atomic precession signal and the digital resonator signal are routed through the gain and phase shift modules and then coupled via an adder. The coupled signal is fed back to both the digital resonator and the atoms. **b**, **c** Simplified model of the hybrid non-Hermitian system and the response before and after coupling. After the AM unit couples with the DE unit, its linear response becomes an EP-enhanced response, with maximum enhancement near the EPs (as indicated by the stars); $\Delta\omega$ is the eigenfrequency difference between atoms and the digital resonator. **d** Experimental results of the system response. The left figure illustrates the response of the AM and the EP-enhanced magnetometer to changes in the DC magnetic field ΔB. ω_0 is the initial frequency of the system response when $\Delta B = 0$. The right figure shows a comparison of their responses to an AC-modulated magnetic field signal $\delta B \bullet \cos(\omega t)$. EP response: The system response when the AM unit is coupled with the DE unit. Non-EP response: The system response when the AM unit is decoupled from the DE unit.

 https://doi.org/10.1038/s41467-026-72864-0

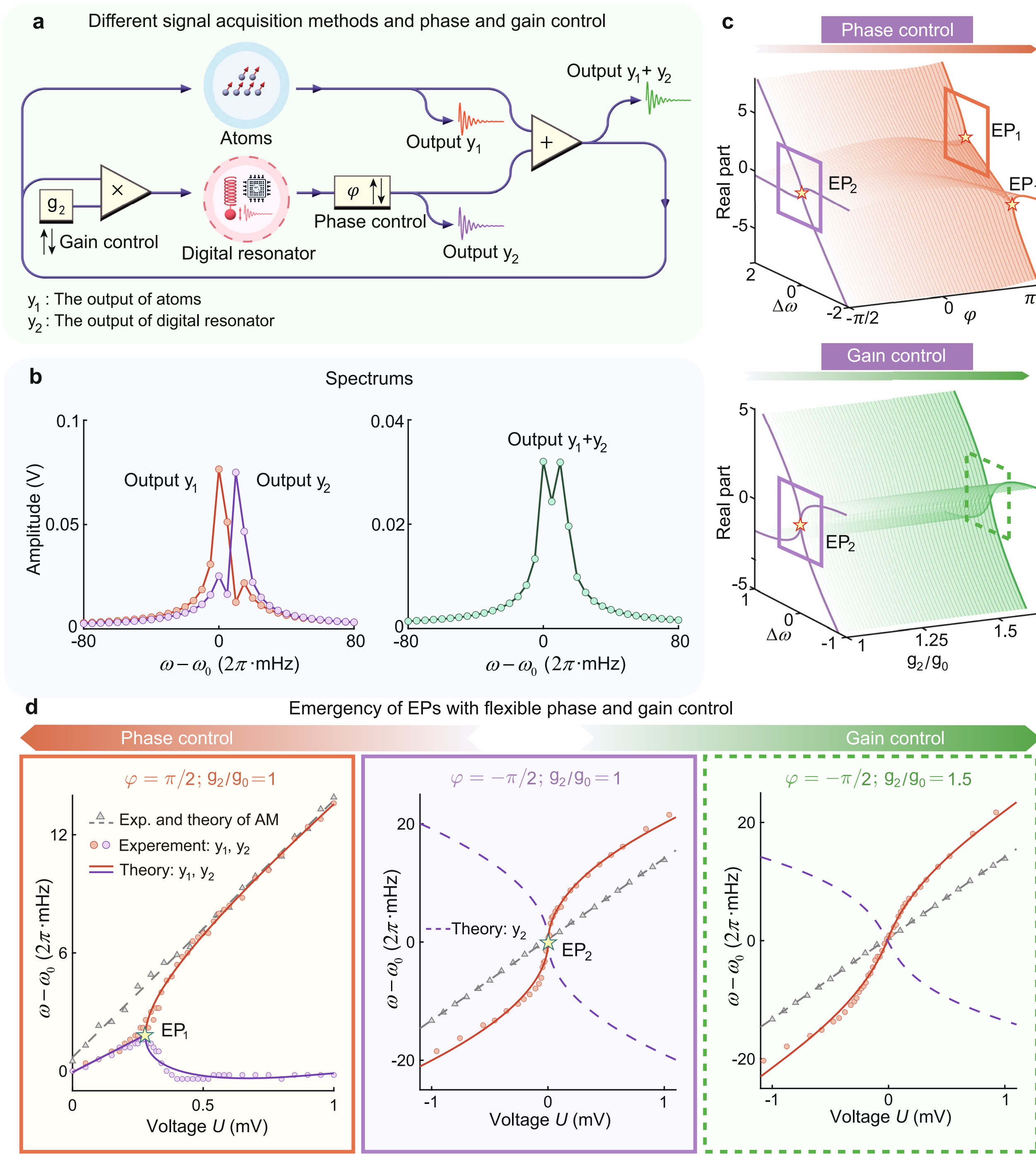

Fig. 2 | Flexible control of the hybrid non-Hermitian magnetometer. a Control and signal extraction procedure for our hybrid non-Hermitian system. The system control consists of gain g_2 and phase φ. The hybrid system can simultaneously acquire three signals: the atomic signal y_1, the digital resonator signal y_2, and the combined signal $y_1 + y_2$, through separate ports. **b** The Fourier spectra of the system output signal. The mutually independent data ports of the digital electronics can be used to separately extract signals from the magnetometer and the digital resonator or to extract the total signal. **c** Dependence of the real parts of the eigenvalues on the phase shift φ and the gain module g_2. **d** Experimental results for φ and g_2 control. The gray triangles represent the signal of the conventional AM, while the orange circles correspond to the magnetometer signal y_1 in the EP-enhanced magnetometer, and the purple circles represent the signal of the digital resonator y_2. The scatter points are experimental signals, and the curves are fits to data. The relationship between the voltage and the magnetic field is $B_z = 1.26\mathrm{nTmV}^{-1} \bullet U$.

In summary, we coupled the AM unit with the DE unit to form a non-Hermitian system. Connected via signal transmission and feedback, the two units still maintain a degree of independence in line with modular design. Thus, the DE unit can also be easily coupled with other sensors. Moreover, the programmability of the digital circuit makes system control more flexible.

Phase and gain control of the system

To more thoroughly investigate the effects of gain and phase control, we regulated the phase shift φ and gain g_2 to manipulate the hybrid system and EPs, with a schematic of the system setup shown in Fig. 2a. Notably, the signal frequencies of the atoms and the digital resonator can separately reflect changes in the eigenvalues of the system. As shown in Fig. 2b, unlike the purely physical system, the hybrid system can simultaneously acquire various signals, including the AM unit signal y_1, the DE unit signal y_2, and the total coupled signal y_1+y_2, which is beneficial for signal extraction and analysis. See Supplementary Fig. 1–4 for the complete signal processing procedure.

Before controlling the phase φ, we normalize the gain modules by setting $\kappa_1=\kappa_2=1$; $g_1=g_2=g_0$ and adjust the loss so that $\gamma_1=\gamma_2=\gamma_0$, which makes the form of the Hamiltonian more concise and clear. When $\theta=\pi/2$ and $\varphi=\pi/2$, the eigenvalues take the form $\lambda_1=i(g_0-\gamma_0)\pm\sqrt{(\Delta\omega^2-g_0^2)}$, and the EPs occur at $\Delta\omega=\pm g_0$. In contrast, when $\theta=\pi/2$ and $\varphi=-\pi/2$, the eigenvalues become $\lambda_2=-i\gamma_0\pm\sqrt{(\Delta\omega^2+2ig_0\Delta\omega)}$, and the EPs occur at $\Delta\omega=0$. As shown in Fig. 2c, as φ varies from $\pi/2$ to $-\pi/2$, the real parts of the eigenvalues transition from a dual-EP state to a single-EP state (Changes in the imaginary parts of the eigenvalues are detailed in the Supplementary Materials.) In the dual-EP state ($\varphi=\pi/2$), the system response increases only when the system is in the PT-symmetry broken phase. In the PT-symmetric phase, the response is weaker than that of the conventional AM. Conversely, in the single-EP state ($\varphi=-\pi/2$), the system response is increased on both sides of the EP.

In addition to phase φ control, control using gain coefficient g_2 can be easily achieved here. As shown in Fig. 2c, taking the single-EP state ($\theta=\pi/2$ and $\varphi=-\pi/2$) as an example, the system's response at $\Delta\omega=0$ gradually decreases from infinity and becomes more linear as g_2 increases from g_0. As a result, the system transitions from an EP-enhanced response to a linear response, indicating gradual decoupling between the atoms and the digital resonator.

In Fig. 2d, by adjusting the voltage U of the B_z coil, we changed the eigenfrequency difference $\Delta\omega$ between the resonators, and measured the system response frequency under different conditions of φ and g_2. As shown in the left and middle panels of Fig. 2d, when the phases are $\theta=\pi/2$ and $\varphi=\pi/2$, a degeneracy exists in the PT-symmetric phase, where the system response is lower than that of a conventional AM; as a result, the sensor response is increased only in the PT-symmetry broken phase. When the phase is changed to $\varphi=-\pi/2$, the system transforms from a dual-EP state to a single-EP state, eliminating the degeneracy at the EP. Thus, the sensor response is increased on both sides of the EP, which is beneficial for practical measurements. We next investigated how regulating the gain coefficient g_2 affects the system. Increasing g_2/g_0 from 1 to 1.5 reduces the system response but significantly increases the linearity of the response (Fig. 2d, middle and right panels). Therefore, during actual measurements, the sensitivity and linear response of the sensor can be balanced by adjusting g_2 according to specific measurement requirements. The experimental results fit well with our theory, highlighting the advantages of the high level of control in our system.

As shown in Fig. 2d, our effective control of phase and gain coefficient confirms that the flexibility of the DE unit makes the regulation of EPs in non-Hermitian systems easier. Also, the figure clearly shows the response enhancement. The slope of the EP-enhanced magnetometer response curve is significantly larger than that of the conventional atomic magnetometer.

EP-enhancement weak magnetic field measurements

To further verify the response and sensitivity enhancement of the system, we applied an AC modulation to B_z and performed measurements using the hybrid non-Hermitian system in both the EP and non-EP states. We measured the system performance under different gain modules g_2 and input signal modulation amplitudes. In the experiments of this work, we use the noise-equivalent magnetic field (NEM) to quantify the sensitivity. The sensitivity is related to the signal-to-noise ratio (SNR) by NEM $\propto 1/\mathrm{SNR}$. Therefore, as shown in Fig. 3, we first measure the response and noise enhancement factors of the system, and then divide the former by the latter to obtain the SNR improvement factor, which is also the sensitivity enhancement factor of the system. (The details are provided in the Supplementary Materials).

We varied g_2 to study how the sensitivity enhancement changes as the system shifts from an EP-enhanced response to a linear response. Adjusting the input amplitude alters both the input signal and noise, allowing us to examine the relationship between sensitivity enhancement and the input signal. When g_2/g_0 approaches 1, the response is increased by a maximum of 4.52 times. As g_2 increases further, the response enhancement decreases because the increasing g_2 disrupts the symmetry between the atoms and the digital resonator, moving the system away from the EP. Moreover, increasing g_2 amplifies the digital resonator feedback signal, introducing more current noise. Consequently, the sensitivity enhancement, which is influenced by both the response and noise enhancements, decreases with increasing g_2, eventually leading to a sensitivity for the hybrid system that is lower than that of the conventional AM. At $g_2/g_0=1$, the sensitivity of the EP-enhanced magnetometer is still increased by 4.27 times, confirming its practicality in magnetic measurement applications.

Next, we increased the input signal amplitude with $g_2/g_0=1$ and evaluated system performance. As shown in Fig. 3b, as the amplitude increased, the response enhancement decreased, the noise enhancement increased, and the sensitivity enhancement decreased. Despite the presence of higher noise than in the previous experiments, the response was increased by a maximum of 4.46 times, and the sensitivity was increased by 3.03 times. This trend reflects the results of the previous experiment. When the input signal becomes stronger, the system response range widens, forcing the system to operate further from the EP, thus weakening the response enhancement. Additionally, a larger input signal carries more noise, which reduces the relative background noise and degrades noise suppression (see **Methods** for details). As the input signal amplitude increases, the sensitivity enhancement eventually decreases below 1. In general, for the EP-enhanced magnetometer, the effects of response enhancement and sensitivity enhancement do exist. Moreover, the closer the system state is to the EPs and the smaller the input signal, the more obvious this effect is.

Discussion

Thanks to the hybrid of physical sensors and digital electronics, our system has many advantages unattainable for the structure based on pure physical systems. Our experimental results show that the DE unit effectively strengthens the response and sensitivity of the AM, which has considerable practical significance. This enhancement relies on the system working near the EP. Unlike purely physical non-Hermitian systems, which are often overly sensitive to the environment, the powerful digital programming of the DE unit enables the system to easily maintain the EPs.

Another advantage of our system is its great programming capability. The digital resonator in the DE unit is fully implemented via computer software, so its physical properties, such as the frequency, loss, and order, can be easily controlled by programming. This not only makes system regulation flexible but also provides the necessary conditions for integrating AI algorithms. The programmability allows the system to overcome limitations on the number of components. Coupling multiple (even dozens of) physical sensors and digital units may thus be feasible. This creates opportunities for studying novel physical phenomena and mechanisms.

The key advantage of our hybrid system is the complete separation of the sensing and DE control units, which is achieved through a plug-in modular design. The sampling frequency of the DE unit can easily reach the GHz level; thus, this design can be extended to several physical systems. For magnetic, optical, or mechanical sensing applications, as long as the sensing unit meets the physical characteristics of

 https://doi.org/10.1038/s41467-026-72864-0

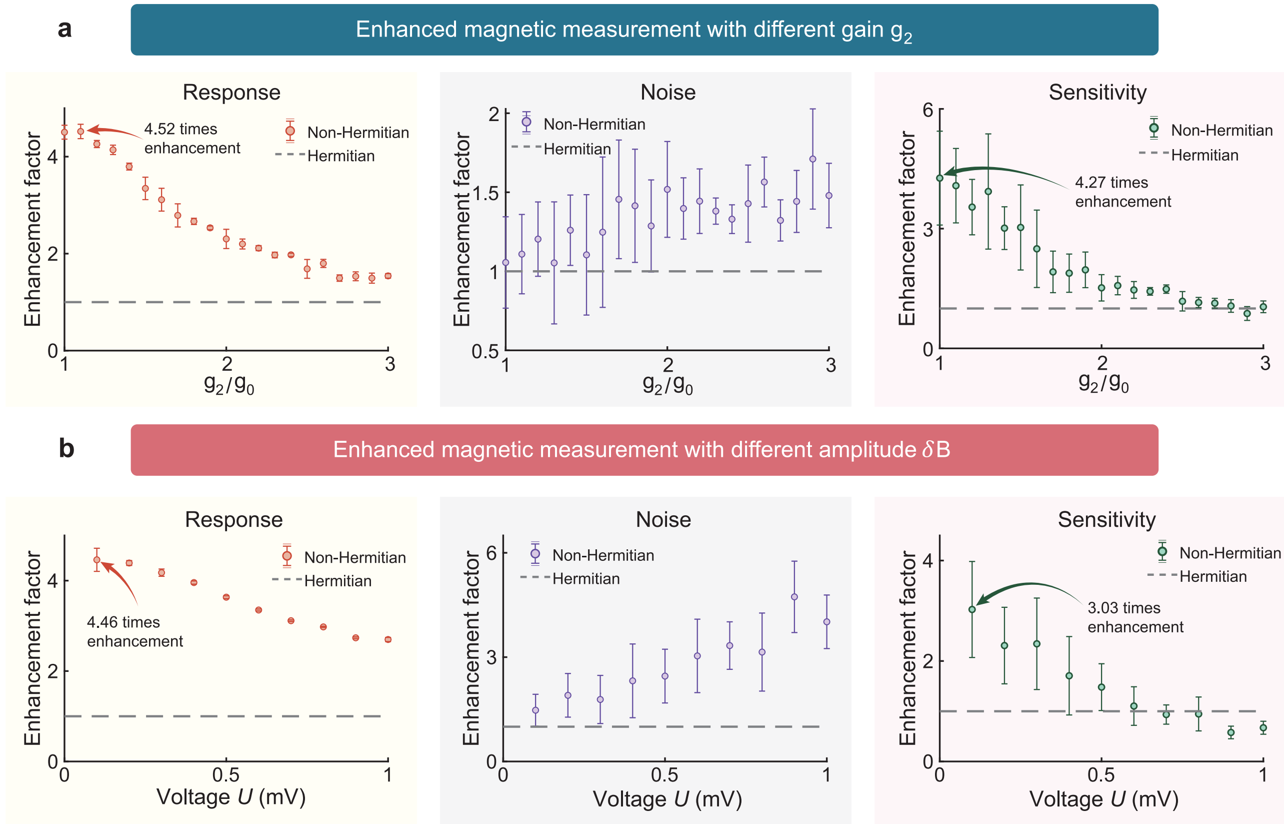

Fig. 3 | EP-enhanced sensitivity of the hybrid magnetometer. Experimental results for the response, noise, and sensitivity under AC modulation $\delta B \bullet \cos(\omega t)$. The data points and error bars represent the mean values and the uncertainty (σ), respectively, obtained from five independent repeated experiments. **a** Response, noise, and sensitivity enhancement results under different g_2 conditions. The gray dashed line represents the measurement results of the AM unit without coupling to the DE unit, so the enhancement factor of it remains at 1. The orange, purple, and green data points represent the measurement results of the AM unit after coupling to the DE unit. When $g_2/g_0 = 1$, the system achieves the best response and sensitivity enhancement. **b** Response, noise, and sensitivity enhancement results under different input signal amplitudes. When the amplitude is 0.1 mV, the system achieves the best enhancement.

a dissipative resonator, it can serve as the sensing unit. Most sensing mechanisms can satisfy the condition of a dissipative resonator. For example, in mechanical sensors, elastic elements under damping exhibit characteristics of a dissipative resonator[52]. Similarly, the voltage or current response in *RLC* circuits[53] and the optical modes within optical cavities[21], when subjected to loss, can also be described via a dissipative resonator model. More importantly, the DE unit serves as an EP generator and is compatible with a linear physical sensor. This fundamentally transforms the physical properties of the sensing unit, enabling the system to shift from Hermitian to non-Hermitian and the emergence of EPs, which is essential for increasing measurement sensitivity. Therefore, this hybrid design could become a link between non-Hermitian theory research and precision measurement applications. In the future, it could find widespread use in both domains.

Furthermore, although we have only demonstrated the sensitivity enhancement for magnetic field measurement by using ^{129}Xe, we believe that using the DE unit to construct other non-Hermitian spin sensors is also feasible. For example, coupling other atoms (such as ^{3}He, Cs, and Rb) with the DE unit can establish corresponding EP-enhanced magnetometers, which are expected to further improve the sensitivity of magnetic field measurement; coupling Xe isotopes (^{129}Xe and ^{131}Xe) with the DE unit can construct an EP-enhanced comagnetometer for improving the system's rotation measurement sensitivity. Overall, thanks to the flexible advantages of the DE unit, our technical solution can meet diverse application requirements.

We have to admit that our current system has limitations, such as the restricted response frequency of digital electronics and the nonlinear effect of atomic magnetometers. But these don't affect the current experimental results and will be our future research directions and priorities.

In conclusion, we proposed a computer-based DE unit that can couple with physical systems to form a combined hybrid non-Hermitian and realize flexible phase and gain control. In experiments, we used this DE unit to construct an EP-enhanced magnetometer and performed highly sensitive magnetic field measurements. Compared with a conventional AM, the EP-enhanced magnetometer achieved increases of up to 4.52 times in response and 4.27 times in sensitivity.

The addition of a suitable DE unit with physical sensors neither obscures the sensors' original physical characteristics nor underutilizes their potential. Instead, it transforms the inherent loss, which has previously been regarded as a detrimental factor to be minimized, into an advantageous feature that amplifies the detection capabilities of such systems.

This work could provide more possibilities and greater intelligence for precision measurement and non-Hermitian research. The DE unit can potentially be used to upgrade traditional sensors to EP-enhanced sensors with higher responses and sensitivity. The DE unit is a flexible and precise experimental platform for studying various physical effects. In the future, we plan to further investigate higher-order EPs[27,54], non-Hermitian topological phenomena[7,53], and nonlinear effects[2,55]. Additionally, we will integrate AI algorithms into hybrid systems to further enhance their performance and explore their applications in the measurement of various physical quantities, such as magnetic fields, electric fields, sound, gravity, and displacement.

Methods

Atomic magnetometer (AM) unit

The AM, constructed using high-temperature ^{87}Rb-^{129}Xe atoms, measures the external magnetic field strength via Larmor precession. The atoms are enclosed in a spherical glass vapor cell with a diameter of about 8 mm, containing 10 Torr of ^{129}Xe, 300 Torr of buffer gas N_2, and an excess of saturated Rb metal. During the experiment, the vapor cell is kept at 105 °C. The relationship between the precession frequency ω_a of the atoms and the external magnetic field B_z is given by $\omega_a = \Gamma B_z$, where Γ is the gyromagnetic ratio, which is approximately 2π•11.86 mHz nT^{-1}. The loss γ is approximately 0.0076 s^{-1}, and the eigenfrequency ω_1 is approximately 161.1 Hz. The coil constant for the B_z magnetic field is approximately 1.26 nT mV^{-1}.

To operate the system, the vapor cell is first heated to vaporize Rb, and then, the Rb atoms are polarized via a pump light source. The pump light has a power of 35.52 mW and a wavelength of 795 nm, corresponding to the D1 line of Rb atoms. The probe light has a power of 1.05 mW and a wavelength of 780 nm, which is detuned by 40 GHz from the D2 line of Rb atoms. The Xe atoms are also polarized via spin exchange optical pumping. Once the preparation is complete, the Xe atoms are excited into a magnetic resonance (a coherent state) via a magnetic field pulse produced by a pulse current through the coil. The precession frequency of Xe is measured by an embedded Rb magnetometer. Over time, the coherent state of the Xe atoms decays due to loss mechanisms, causing the signal to weaken and eventually disappear.

Digital electronic (DE) unit

We use the first-order Butterworth band-pass filter module in LabVIEW to implement the digital resonator. This module can readily simulate the signal and response of the resonator, and by changing the bandwidth and center frequency, we can correspondingly vary the loss and eigenfrequency of the DE unit. In the experiment, a 7856 R FPGA board is additionally used for sampling, with a sampling rate of 500 kHz.

To ensure that the system state passes through the EP, the magnetometer and digital resonator must be symmetric, so the loss and frequency of the digital resonator are matched to those of the Xe atoms. Then, we compensate for phase shifts caused by signal transmission, setting $\theta = \pi/2$ and $\varphi = \pi/2$, and adjust the gain modules to satisfy $\kappa_1 = \kappa_2 = 1$; $g_1 = g_2 = g_0$, which are easily achieved through programming.

Phase and gain control

Under the conditions $\kappa_1 = \kappa_2 = 1$ and $g_1 = g_2 = g_0$, when the phase θ and φ vary, the system's Hamiltonian and eigenvalues change, leading to changes in the system's behavior near the EP. When $\theta = \pi/2, \varphi = \pi/2$, the system is in a dual-EP state, and the Hamiltonian becomes:

$$\widehat{H}_{eff} = \begin{pmatrix} \Delta\omega - i\gamma_0 + ig_0 & ig_0 \\ ig_0 & -\Delta\omega - i\gamma_0 + ig_0 \end{pmatrix}. \tag{6}$$

When $\theta = \pi/2, \varphi = -\pi/2$, the system is in a single-EP state, and the Hamiltonian becomes:

$$\widehat{H}_{eff} = \begin{pmatrix} \Delta\omega - i\gamma_0 + ig_0 & -ig_0 \\ ig_0 & -\Delta\omega - i\gamma_0 - ig_0 \end{pmatrix}. \tag{7}$$

In the dual-EP state, the degeneracy of the eigenvalues can cause a reduced response during measurement.

Starting from the single-EP configuration, gain control can change the response characteristics of the system. When g_2/g_0 is no longer fixed at 1, the expression for the eigenvalues is as follows:

$$\lambda = \frac{1}{2}\left(-i\gamma_0 + ig_0 - ig_2 \pm \sqrt{(2\Delta\omega + ig_0 + ig_2)^2 + 4g_0 g_2}\right). \tag{8}$$

By adjusting g_2, we shift the system away from the EP, modifying the response zero-crossing slope and linearity. The response enhancement is related to the slope of the real part of the eigenvalue:

$$\left.\frac{\partial\lambda(Re)}{\partial\omega}\right|_{(\Delta\omega=0)} = \left|\frac{g_0 + g_2}{g_0 - g_2}\right|. \tag{9}$$

According to this equation, when $g_2/g_0 > 1$ (or $g_2/g_0 < 1$), the response amplification decreases. When $g_2/g_0 \to +\infty$ (or $g_2/g_0 \to 0$), the slope of the real part of the eigenvalue approaches 1. Therefore, as g_2 increases (or decreases), the system response shifts from sublinear to linear, with linearity increasing gradually.

Noise analysis

To better understand the improved sensitivity, it is necessary to focus on the variation of system noise before and after coupling. As the response near the EP is enhanced, the input signal noise is amplified, but the background noise is not. The input signal can be split into a useful signal part S_I and a noise part N_I. Let the response enhancement of the original sensor be g_a, and let the response enhancement of the EP-enhanced sensor be g_{ad}. The outputs of the original sensor Y_a and the EP-enhanced sensor Y_{ad} are as follows:

$$\begin{aligned} Y_a &= \sqrt{g_a^2 S_I^2 + g_a^2 N_I^2 + N_a^2} \\ Y_{ad} &= \sqrt{g_{ad}^2 S_I^2 + g_{ad}^2 N_I^2 + N_{ad}^2} \end{aligned}, \tag{10}$$

where N_a and N_{ad} are the noise floors of the original and EP-enhanced sensors, respectively. Assuming that $g_a = 1$, we have:

$$Y_a = \sqrt{S_I^2 + N_I^2 + N_a^2}. \tag{11}$$

The response, noise, and sensitivity enhancement of the EP-enhanced sensor are compared with those of the original sensor.

The response enhancement of the two sensors is compared as follows:

$$g_r = \frac{S_I g_{ad}}{S_I} = g_{ad}. \tag{12}$$

The noise enhancement of the two sensors is compared as follows:

$$g_n = \frac{\sqrt{g_{ad}^2 N_I^2 + N_{ad}^2}}{\sqrt{N_I^2 + N_a^2}}. \tag{13}$$

The sensitivity enhancement of the two sensors is compared as follows:

$$g_{SNR} = g_{ad}\frac{\sqrt{N_I^2 + N_a^2}}{\sqrt{g_{ad}^2 N_I^2 + N_{ad}^2}}. \tag{14}$$

As g_{ad} increases, the sensitivity enhancement improves, approaching:

$$\lim_{g_{ad}\to\infty} g_{SNR} = \sqrt{1 + \left(\frac{N_a}{N_I}\right)^2}. \tag{15}$$

This shows that a higher background noise N_a of the original sensor makes the non-Hermitian system more advantageous. Thus, the main advantage of the EP-enhanced sensor is that it suppresses background noise.

The noise sources of an atomic magnetometer can be divided into three main categories: quantum noise, environmental noise, and technical noise. Quantum noise includes spin-projection noise, photon shot noise, and AC-Stark–shift–associated noise. In general, these all belong to N_a, i.e., the background noise. Environmental noise mainly consists of thermal noise and magnetic-field noise. In practical measurements, thermal noise is essentially independent of the signal strength to be measured and therefore belongs to N_a, whereas magnetic-field noise is amplified together with the signal after it is input into the system and thus belongs to N_I. Technical noise involves a wide variety of contributing factors, including laser, detector, electronic, and mechanical noise. These noises are distributed over all stages of the sensing process and are related to the hardware configuration. Consequently, part of them arises in the coupling stage of the system, and another part is introduced together with the input signal, contributing to N_a and N_I, respectively.

Data availability

Source data have been deposited in the Figshare database and are publicly available for this paper (https://doi.org/10.6084/m9.figshare.29433827). All other data that support the plots within this paper and other findings of this study are available from the corresponding authors upon request.

References

1. Zhao, H. & Feng, L. Parity–time symmetric photonics. *Natl. Sci. Rev.* **5**, 183–199 (2018).
2. Roy, A. et al. Nondissipative non-hermitian dynamics and exceptional points in coupled optical parametric oscillators. *Optica* **8**, 415–421 (2021).
3. Tang, Y. et al. PT-Symmetric Feedback Induced Linewidth Narrowing. *Phys. Rev. Lett.* **130**, 193602 (2023).
4. Deng, W., Zhu, W., Chen, T., Sun, H. & Zhang, X. Ultrasensitive integrated circuit sensors based on high-order non-Hermitian topological physics. *Sci. Adv.* **10**, eadp6905 (2024).
5. Wu, X. et al. Studying Quasi-Parametric Amplifications: From Multiple PT-Symmetric Phase Transitions to Non-Hermitian Sensing. *ACS Photonics* **11**, 4662–4670 (2024).
6. Peng, J.-X., Zhu, B., Zhang, W. & Zhang, K. Enhanced Quantum Metrology with Non-Phase-Covariant Noise. *Phys. Rev. Lett.* **133**, 090801 (2024).
7. Parto, M., Leefmans, C., Williams, J., Gray, R. M. & Marandi, A. Enhanced sensitivity via non-Hermitian topology. *Light Sci. Appl.* **14**, 6 (2025).
8. Heiss, W. D. The physics of exceptional points(Article). *J. Phys. A: Math. Theor.* **45**, 444016 (2012).
9. Wiersig, J. Review of exceptional point-based sensors. *Photonics Res.* **8**, 1457–1467 (2020).
10. McDonald, A. & Clerk, A. A. Exponentially-enhanced quantum sensing with non-Hermitian lattice dynamics. *Nat. Commun.* 1–12 (2020).
11. Peters, K. J. H. & Rodriguez, S. R. K. Exceptional precision of a nonlinear optical sensor at a square-root singularity. *Phys. Rev. Lett.* **129**, 013901 (2022).
12. Özdemir, ŞK., Rotter, S., Nori, F. & Yang, L. Parity–time symmetry and exceptional points in photonics. *Nat. Mater.* **18**, 783–798 (2019).
13. Hokmabadi, M. P., Schumer, A., Christodoulides, D. N. & Khajavikhan, M. Non-Hermitian ring laser gyroscopes with enhanced Sagnac sensitivity. *Nature* **576**, 70–74 (2019).
14. Liang, C., Tang, Y., Xu, A.-N. & Liu, Y.-C. Observation of exceptional points in thermal atomic ensembles. *Phys. Rev. Lett.* **130**, 263601 (2023).
15. Li, Z., Prasad, C. S., Wang, X., Zhang, D. & Naik, G. V. Sensing beyond the exceptional point for high detectivity. *ACS Photonics* **11**, 2954–2960 (2024).
16. Bao, L., Qi, B., Nori, F. & Dong, D. Exponential sensitivity revival of noisy non-Hermitian quantum sensing with two-photon drives. *Phys. Rev. Res.* **6**, 023216 (2024).
17. Hodaei, H. et al. Enhanced sensitivity at higher-order exceptional points. *Nature* **548**, 187–191 (2017).
18. Sunada, S. Large Sagnac frequency splitting in a ring resonator operating at an exceptional point. *Phys. Rev. A* **96**, 033842 (2017).
19. Lai, Y.-H., Lu, Y.-K., Suh, M.-G., Yuan, Z. & Vahala, K. Observation of the exceptional-point-enhanced Sagnac effect. *Nature* **576**, 65–69 (2019).
20. Zhang, H. et al. Breaking anti-PT symmetry by spinning a resonator. *Nano Lett.* **20**, 7594–7599 (2020).
21. Arkhipov, I. I., Miranowicz, A., Minganti, F. & Nori, F. Quantum and semiclassical exceptional points of a linear system of coupled cavities with losses and gain within the Scully-Lamb laser theory. *Phys. Rev. A* **101**, 013812 (2020).
22. Qin, G. Q. et al. Experimental realization of sensitivity enhancement and suppression with exceptional surfaces. *Laser Photonics Rev.* **15**, 1–6 (2021).
23. Chowdhury, B. N., Lahiri, P., Johnson, N. P., de la Rue, R. M. & Lahiri, B. Exceptional-point-enhanced superior sensing using asymmetric coupled-lossy-resonator based optical metasurface. *Laser Photonics Rev.* **19**, 1 (2024).
24. Quijandría, F., Naether, U., Özdemir, S. K., Nori, F. & Zueco, D. P. T.-symmetric circuit QED. *Phys. Rev. A* **97**, 053846 (2018).
25. Dong, Z., Li, Z., Yang, F., Qiu, C.-W. & Ho, J. S. Sensitive readout of implantable microsensors using a wireless system locked to an exceptional point. *Nat. Electron.* **2**, 335–342 (2019).
26. Hajizadegan, M., Sakhdari, M., Liao, S. & Chen, P.-Y. High-sensitivity wireless displacement sensing enabled by PT-symmetric Telemetry. *IEEE Trans. Antennas Propag.* **67**, 3445–3449 (2019).
27. Xiao, Z., Li, H., Kottos, T. & Alù, A. Enhanced sensing and non-degraded thermal noise performance based on PT-symmetric electronic circuits with a sixth-order exceptional point. *Phys. Rev. Lett.* **123**, 213901 (2019).
28. Bai, K. et al. Nonlinearity-enabled higher-order exceptional singularities with ultra-enhanced signal-to-noise ratio. *Natl. Sci. Rev.* **10**, 98–106 (2023).
29. Park, J.-H. et al. Symmetry-breaking-induced plasmonic exceptional points and nanoscale sensing. *Nat. Phys.* **16**, 462–468 (2020).
30. Zhou, X. et al. Higher-order singularities in phase-tracked electromechanical oscillators. *Nat. Commun.* **14**, 7944 (2023).
31. Zhao, H., Chen, Z., Zhao, R. & Feng, L. Exceptional point engineered glass slide for microscopic thermal mapping. *Nat. Commun.* **9**, 1764 (2018).
32. Zhang, X., Hu, J. & Zhao, N. Stable atomic magnetometer in parity-time symmetry broken phase. *Phys. Rev. Lett.* **130**, 023201 (2023).
33. Kononchuk, R., Cai, J., Ellis, F., Thevamaran, R. & Kottos, T. Exceptional-point-based accelerometers with enhanced signal-to-noise ratio. *Nature* **607**, 697–702 (2022).
34. Huang, R. et al. Exceptional photon blockade: engineering photon blockade with chiral exceptional points. *Laser Photonics Rev.* **16**, 2100430 (2022).
35. He, W. et al. Loss-enabled chirality inversion in terahertz metasurfaces. *Phys. Rev. Lett.* **134**, 106901 (2025).
36. Wan, S. et al. Spin-selective topological effects without encircling exceptional points. *Phys. Rev. Lett.* **136**, 053801 (2026).
37. Feng, L., El-Ganainy, R. & Ge, L. Non-Hermitian photonics based on parity–time symmetry. *Nat. Photonics* **11**, 752–762 (2017).
38. Chen, C., Jin, L. & Liu, R. Sensitivity of parameter estimation near the exceptional point of a non-Hermitian system(Article). *N. J. Phys.* **21**, 083002 (2019).
39. Wang, H., Lai, Y.-H., Yuan, Z., Suh, M.-G. & Vahala, K. Petermann-factor sensitivity limit near an exceptional point in a Brillouin ring laser gyroscope. *Nat. Commun.* **11**, 1–6 (2020).

40. Carlo, M. D., Leonardis, F. D., Soref, R. A. & Passaro, V. M. N. Design of an exceptional-surface-enhanced silicon-on-insulator optical accelerometer. *J. Lightwave Technol.* **39**, 5954–5961 (2021).
41. Zhang, G.-Q. et al. Exceptional Point And Cross-relaxation Effect In A Hybrid Quantum System. *PRX Quantum* **2**, 020307 (2021).
42. Ruan, Y.-P. et al. Observation of loss-enhanced magneto-optical effect. *Nat. Photonics* **19**, 109–115 (2025).
43. Xu, J. et al. Single-cavity loss-enabled nanometrology. *Nat. Nanotechnol.* **19**, 1472–1477 (2024).
44. Langbein, W. No exceptional precision of exceptional-point sensors. *Phys. Rev. A* **98**, 023805 (2018).
45. Lau, H.-K. & Clerk, A. A. Fundamental limits and non-reciprocal approaches in non-Hermitian quantum sensing. *Nat. Commun.* **9**, 4320 (2018).
46. Mortensen, N. A. et al. Fluctuations and noise-limited sensing near the exceptional point of parity-time-symmetric resonator systems. *Optica* **5**, 1342–1346 (2018).
47. Bao, L., Qi, B., Dong, D. & Nori, F. Fundamental limits for reciprocal and nonreciprocal non-Hermitian quantum sensing. *Phys. Rev. A* **103**, 042418 (2021).
48. Ding, W., Wang, X. & Chen, S. Fundamental sensitivity limits for non-Hermitian quantum sensors. *Phys. Rev. Lett.* **131**, 160801 (2023).
49. Reisenbauer, M. et al. Non-Hermitian dynamics and non-reciprocity of optically coupled nanoparticles. *Nat. Phys.* **20**, 1629–1635 (2024).
50. Xie, H. & Fedder, G. K. Integrated microelectromechanical Gyroscopes. *J. Aerosp. Eng.* **16**, 65–75 (2003).
51. Wu, Y. et al. Third-order exceptional line in a nitrogen-vacancy spin system. *Nat. Nanotechnol.* **19**, 160–165 (2024).
52. Chen, Y., Li, X., Scheibner, C., Vitelli, V. & Huang, G. Realization of active metamaterials with odd micropolar elasticity. *Nat. Commun.* 5935 (2021).
53. Yuan, H. et al. Non-Hermitian topolectrical circuit sensor with high sensitivity. *Adv. Sci.* **10**, 2301128 (2023).
54. Li, Z.-Z., Chen, W., Abbasi, M., Murch, K. W. & Whaley, K. B. Speeding Up Entanglement Generation by Proximity to Higher-Order Exceptional Points. *Phys. Rev. Lett.* **131** (2023). https://doi.org/10.1103/PhysRevLett.131.100202
55. Zheng, X. & Chong, Y. D. Noise constraints for nonlinear exceptional point sensing. *Phys. Rev. Lett.* **134**, 133801 (2025).

Acknowledgements
The authors are grateful to Chengzhi Hou, Zhixian Liu, Ye Geng, and Wei Liu for fruitful discussions. H.J. is supported by the National Key R&D Program of China (Grant No. 2024YFE0102400), the National Natural Science Foundation of China (Grants nos. 11935006 and 12421005), and the Hunan Major Sci-Tech Program (Grant no. 2023ZJ1010). Z.W. is supported by the National Natural Science Foundation of China (Grant nos. U23B2066 and 12174446), the Hunan Provincial Natural Science Foundation of China for Distinguished Young Scholars (Grant no. 2023JJ10050), and the Innovation Research Foundation of National University of Defense Technology. J.X. is supported by the National Natural Science Foundation of China (Grant no. 62505360) and the National University of Defense Technology Foundation (Grant no. ZK25-40). R.H. is supported by the RIKEN Special Postdoctoral Researchers (SPDR) program. F. N. is supported in part by the Japan Science and Technology Agency (JST) [via the CREST Quantum Frontiers program Grant No. JPMJCR24I2, the Quantum Leap Flagship Program (Q-LEAP), and the Moonshot R&D Grant no. JPMJMS256E]. K.X. is supported by the National Natural Science Foundation of China (Grant Nos. 92365107 and U25A6008), the Innovation Program for Quantum Science and Technology (Grant no. 2021ZD0301400), and the Innovation Research Foundation of National University of Defense Technology (Grant no. 24-ZZCX-JDZ-11).

Author contributions
T.Q. and J.X. jointly contributed to the study as co-first authors. T.Q., J.X., R.H., K.X., F.N., H.J., and Z.W. conceived the idea. T.Q., Z.X., H.Z., C.W., J.L., J.Z., and Z.W. conducted the experiments and analyzed the data together with all the other authors. T.Q., J.X., R.H., H.L., S.Q., F.N., H.J., and Z.W. wrote the manuscript with contributions from all the other authors.

Competing interests
The authors declare no competing interests.

Additional information
Supplementary information The online version contains supplementary material available at https://doi.org/10.1038/s41467-026-72864-0.

Correspondence and requests for materials should be addressed to Hui Luo, Shiqiao Qin, Hui Jing or Zhiguo Wang.

Peer review information *Nature Communications* thanks Yong-Chun Liu and Lucas Rushton for their contribution to the peer review of this work. A peer review file is available.